

Multi-flavor massless QED₂ at finite densities via Lefschetz thimbles

Yuya Tanizaki^a Motoi Tachibana^b

^a*RIKEN BNL Research Center, Brookhaven National Laboratory, Upton, NY 11973-5000 USA*

^b*Department of Physics, Saga University, Saga 840-8502, Japan*

E-mail: yuya.tanizaki@riken.jp, motoi@cc.saga-u.ac.jp

ABSTRACT: We consider multi-flavor massless (1 + 1)-dimensional QED with chemical potentials at finite spatial length and the zero-temperature limit. Its sign problem is solved using the mean-field calculation with complex saddle points.

Contents

1	Introduction	1
2	(1 + 1)-dimensional massless QED	2
2.1	Setup of the model	2
2.2	Fermion determinant with nontrivial holonomies	4
3	Mean-field approximation with complex saddle points	6
3.1	Lefschetz-thimble methods and mean-field approximation	6
3.2	Charge and complex conjugation for real-valued free energy	7
4	Lefschetz-thimble calculus for multi-flavor massless QED₂	8
4.1	Complex saddle points of multi-flavor massless QED ₂	8
4.2	1-flavor case	10
4.3	2-flavor case	11
4.4	3-flavor case	12
5	Gradient flow inside CK-invariant space	15
6	Conclusion and perspective	17

1 Introduction

Path integral formalism has been used in a wide range to study systems of quantum field theory as well as statistical mechanics. The formalism is useful not only for the perturbative calculations but also for the numerical computations such as the lattice Monte Carlo simulations. However, it is well known that the lattice Monte Carlo simulation does not work when the action of the system becomes complex and this is called the sign problem [1, 2]. It is a big obstacle when we try to compute the high-density nuclear matter based on quantum chromodynamics (QCD) [3].

In this paper, we consider (1 + 1)-dimensional quantum electrodynamics (QED₂) with N_f massless fermions, which we call multi-flavor massless QED₂. It is also known as Schwinger model, which is exactly solvable and mapped to the theory of free massive photons [4, 5]. This model has the sign problem at finite temperature and finite number densities, but its phase structure is studied analytically by Refs. [6–8]. Therefore, multi-flavor massless QED₂ has been used for the test of various approaches to the sign problem; the dual formulation is discussed in Ref. [9], and the study with matrix product states is used for two-flavor massless and massive QED₂ in Ref. [10]. Here, we apply the Lefschetz-thimble method to obtain phase diagram of multi-flavor massless QED₂, and study its property about the sign problem.

The Lefschetz-thimble method was originally developed to study the hyperasymptotic behavior of exponential integrals [11–13], and it was utilized in study of Cherns-Simons theory by Witten [14–16]. Hyperasymptotics is a branch of the resurgence theory, and its application to semiclassical analysis has been recently discussed extensively [17–32]. Lefschetz thimble is the higher-dimensional generalization of steepest descent paths, and it has been applied to the sign problem [33–55]. In this method, complex saddle points of the action play an important role, and the saddle-point approximation with complex saddles describes the essence of nonperturbative behaviors in some cases; it is used for the pair creation under strong laser pulse in Refs. [56–58], and complex saddles also describe the strongly-coupled phase of the Gross–Witten–Wadia model [59, 60].

Using Lefschetz thimbles, we show that mean-field calculation with complex saddles becomes exact in multi-flavor massless QED₂ at finite spacial length and the zero-temperature limit. We identify all the complex saddle points of QED₂ at finite chemical potentials, and draw the phase diagram using that information. At that stage, we must know the intersection numbers between dual thimbles and the original integration region, and those quantities are identified by solving the gradient flow equation that defines Lefschetz thimbles. This is the first non-trivial example of gauge theories with the sign problem that is completely solved by the Lefschetz-thimble method.

This paper is organized as follows. In Section 2, we review the computation of massless QED₂. In Section 3, we explain the mean-field approximation in the presence of the sign problem. In Section 4, we compute the complex saddle points and obtain the phase structures concretely for one-, two-, and three-flavor cases. To discuss the phase structure for three-flavor case, however, we need the intersection numbers. For that purpose, we numerically solve the gradient flow and visualize its structure in Section 5. We summarize our result and discuss some perspectives in Section 6.

2 (1 + 1)-dimensional massless QED

In this section, we review the computation of the massless QED₂. This section does not present a new result, and the main purpose is to set the notation and make the paper self-contained.

2.1 Setup of the model

Let us first consider the path-integral expression of multi-flavor massless QED₂ on a two-dimensional torus $T^2 = [0, \beta] \times [0, L]$. The theory is defined by

$$Z(\beta, L, \mu) = \int \mathcal{D}A e^{-S_{\text{Maxwell}}[A]} \int \mathcal{D}\bar{\psi} \mathcal{D}\psi \exp \left(- \sum_{a=1}^{N_f} \int d^2x \bar{\psi}_a [\not{D}_A - \mu_a \gamma^0] \psi_a \right). \quad (2.1)$$

Here, $A = A_\mu dx^\mu$ is the $U(1)$ gauge field, ψ_a and $\bar{\psi}_a$ are two-component spinor fields with the flavor index $a = 1, \dots, N_f$, $\not{D}_A = \gamma_\nu (\partial_\nu + iA_\nu)$ with Gamma matrices γ_ν , and μ_a is the chemical potentials for fermion number densities $n_a = \bar{\psi}_a \gamma_0 \psi_a$. S_{Maxwell} is the Maxwell

action,

$$S_{\text{Maxwell}}[A] = \frac{1}{4e^2} \int d^2x (\partial_\mu A_\nu - \partial_\nu A_\mu)^2. \quad (2.2)$$

The theory is now defined on the torus $T^2 = [0, \beta] \times [0, L]$ with the thermal boundary condition, i.e.,

$$A_\nu(x^0 + n\beta, x^1 + mL) \sim A_\nu(x^0, x^1), \quad (2.3)$$

$$\psi(x^0 + n\beta, x^1 + mL) = (-1)^n \psi(x^0, x^1). \quad (2.4)$$

The “ \sim ” in the first equation means that the difference between both sides must be appropriately Dirac quantized.

We review the computation of the Dirac operator on the torus T^2 according to Ref. [61]. We decompose the gauge field as

$$A = \left(\frac{2\pi k}{\beta L} x^1 + \frac{2\pi}{\beta} h_0 \right) dx^0 + \frac{2\pi}{L} h_1 dx^1 + *d\phi + d\lambda. \quad (2.5)$$

The meaning of each variables is as follows: λ is a gauge parameter, so it does not affect the computation of physical quantities, such as the partition function. ϕ is a 2π -periodic function on torus without the zero-momentum mode, which represents the local fluctuation of the photon field. Since $F_{01} = -2\pi k/\beta L + \Delta\phi$, the Maxwell action becomes

$$S_{\text{Maxwell}} = \frac{1}{2e^2} \int_{T^2} d^2x \left(\Delta\phi - \frac{2\pi k}{\beta L} \right)^2. \quad (2.6)$$

The fields h_0 and h_1 are sometimes called toron fields: they do not create the electric field, but describe the nontrivial holonomy at $\phi = 0$ and $k = 0$, since

$$\exp \left(i \int_{\mathcal{C}} A \right) \Big|_{\phi=0, k=0} = e^{2\pi i(n_0 h_0 + n_1 h_1)}, \quad (2.7)$$

where n_0 and n_1 are the number of the windings of the closed curve \mathcal{C} along x^0 - and x^1 -directions of T^2 , respectively ($0 \leq h_\mu < 1$). The integer k refers the Chern number,

$$\frac{1}{2\pi} \int_{T^2} dA = -k, \quad (2.8)$$

which creates the constant electric field. The index theorem tells us that k represents the index of the Dirac operator, and thus we need to take into account only the $k = 0$ sector: otherwise, the Dirac zero modes exist and the fermion determinant becomes zero because the fermions are massless.

Let us restrict ourselves to the case $k = 0$ in the following, and assume that the Dirac zero mode does not exist. For simplicity of the computation, we put $\lambda = 0$ by gauge fixing. By putting

$$\tilde{A} = \frac{2\pi}{\beta} h_0 dx^0 + \frac{2\pi}{L} h_1 dx^1, \quad (2.9)$$

we get $A = \tilde{A} + *d\phi$. We define the chirality matrix by $\gamma = -i\gamma^0\gamma^1$, then

$$\mathcal{D}_A = e^{-\gamma\phi} \mathcal{D}_{\tilde{A}} e^{-\gamma\phi}. \quad (2.10)$$

Therefore, we obtain that

$$\det(\not{D}_A) = \det(\not{D}_{\tilde{A}}) \exp\left(-\frac{1}{2\pi} \int d^2x \phi(-\Delta\phi)\right). \quad (2.11)$$

In order to obtain this result, we perform the chiral rotation $\psi \mapsto e^{\gamma\phi}\psi$ and $\bar{\psi} \mapsto \bar{\psi}e^{\gamma\phi}$, and use the anomaly equation. It is important to notice that the global fluctuations \tilde{A} and the local fluctuation ϕ decouple completely from one another at the $k = 0$ sector, thanks to the absence of the Dirac zero modes. Now, the partition function reads

$$\begin{aligned} Z(\beta, L, \mu) &= \int_0^1 dh_0 dh_1 \prod_{a=1}^{N_f} \det(\not{D}_{\tilde{A}} - \mu_a \gamma^0) \\ &\times \int \mathcal{D}\phi \exp\left(-\frac{1}{2e^2} \int d^2x \phi \left(-\Delta + N_f \frac{e^2}{\pi^2}\right) (-\Delta)\phi\right). \end{aligned} \quad (2.12)$$

The photon field ϕ becomes massive due to the chiral anomaly, and it decouples from the integration of h_0 and h_1 fields. In this paper, we are interested only in the dependence on the chemical potentials, and the h_0 and h_1 integrations are most important. In the following, we simply denote that

$$Z(\beta, L, \mu) = \int_0^1 dh_0 dh_1 \prod_{a=1}^{N_f} \det(\not{D}_{\tilde{A}} - \mu_a \gamma^0). \quad (2.13)$$

In the next subsection, we will compute the fermion determinant under the background with nontrivial holonomies.

2.2 Fermion determinant with nontrivial holonomies

One can compute the Dirac determinant in a way to keep the global-gauge invariance manifestly by using the zeta-function regularization (see Ref. [61] and also Appendix in Ref. [62]). To understand the formula intuitively, we derive the result for the fermion determinant heuristically by considering the fermion spectrum. After the chiral transformation, the fermion operator becomes

$$\gamma_0 \not{D}_{\tilde{A}} = \left(\partial_\tau + \frac{2\pi i}{\beta} h_0\right) \mathbf{1}_2 + i \left(\partial_1 + \frac{2\pi i}{L} h_1\right) \gamma, \quad (2.14)$$

where $\gamma = -i\gamma_0\gamma_1$ and in the chiral notation $\gamma = \sigma_3$. Therefore, the spectrum of this operator can be labeled as

$$\frac{2\pi}{L}(n \pm h_1) + \frac{2\pi i}{\beta} h_0 + \frac{(2m+1)\pi i}{\beta}. \quad (2.15)$$

By performing the summation over Matsubara frequencies m , we obtain the Fermi-Dirac distribution for each fermionic mode:

$$1 + \exp\left[-\frac{2\pi\beta}{L}(n \pm h_1) - 2\pi i h_0\right]. \quad (2.16)$$

Contribution of the positive chiral fermions gives

$$\left(1 + e^{-\frac{2\pi\beta}{L}(n+h_1-1)-2\pi i h_0}\right) \left(1 + e^{-\frac{2\pi\beta}{L}(n-h_1)+2\pi i h_0}\right), \quad (2.17)$$

and that of the negative chiral fermions gives

$$\left(1 + e^{-\frac{2\pi\beta}{L}(n+h_1-1)+2\pi i h_0}\right) \left(1 + e^{-\frac{2\pi\beta}{L}(n-h_1)-2\pi i h_0}\right). \quad (2.18)$$

Each term is invariant under $h_0 \mapsto h_0 + 1$, but it is not the case for $h_1 \mapsto h_1 + 1$. Even after taking the product over all spatial momenta $n = 1, 2, \dots$, the invariance under the spatial global gauge transformation is lost by

$$e^{-\frac{2\pi\beta}{L}(-h_1)+2\pi i h_0} e^{-\frac{2\pi\beta}{L}(-h_1)-2\pi i h_0} = e^{\frac{4\pi\beta}{L}h_1}. \quad (2.19)$$

To compensate this factor, one should multiply

$$e^{-\frac{2\pi\beta}{L}(h_1^2-h_1)}. \quad (2.20)$$

We introduce the dimensionless chemical potential μ' and the dimensionless temperature τ by

$$\mu' = \frac{L\mu}{2\pi}, \quad \tau = \frac{L}{\beta}. \quad (2.21)$$

The μ' -dependence of each determinant becomes

$$\begin{aligned} \det(\not{D}_{\tilde{A}} - \mu\gamma_0) &= e^{-\frac{2\pi}{\tau}(h_1^2-h_1)} \prod_{n=1}^{\infty} \left\{ \left(1 + e^{-\frac{2\pi}{\tau}(n+h_1-1-\mu')-2\pi i h_0}\right) \left(1 + e^{-\frac{2\pi}{\tau}(n-h_1+\mu')+2\pi i h_0}\right) \right. \\ &\quad \left. \times \left(1 + e^{-\frac{2\pi}{\tau}(n+h_1-1+\mu')+2\pi i h_0}\right) \left(1 + e^{-\frac{2\pi}{\tau}(n-h_1-\mu')-2\pi i h_0}\right) \right\}. \end{aligned} \quad (2.22)$$

This matches with the correct formula derived in Ref. [61] up to an uninteresting field-independent factor. We define the dimensionless mean-field free energy F by

$$F(h_0, h_1) = -\frac{\tau}{2\pi} \sum_{a=1}^{N_f} \ln \det \left(\not{D}_{\tilde{A}} - \frac{2\pi}{L} \mu'_a \gamma_0 \right). \quad (2.23)$$

The explicit form of this one-loop effective potential becomes

$$\begin{aligned} F &= N_f \left(h_1 - \frac{1}{2} \right)^2 \\ &\quad - \frac{\tau}{2\pi} \sum_{a=1}^{N_f} \sum_{n=1}^{\infty} \left\{ \ln \left(1 + e^{-\frac{2\pi}{\tau}(n+h_1-1-\mu'_a)-2\pi i h_0} \right) + \ln \left(1 + e^{-\frac{2\pi}{\tau}(n-h_1+\mu'_a)+2\pi i h_0} \right) \right. \\ &\quad \left. + \ln \left(1 + e^{-\frac{2\pi}{\tau}(n+h_1-1+\mu'_a)+2\pi i h_0} \right) + \ln \left(1 + e^{-\frac{2\pi}{\tau}(n-h_1-\mu'_a)-2\pi i h_0} \right) \right\}. \end{aligned} \quad (2.24)$$

Using this one-loop effective potential, (2.13) becomes

$$Z = \int_0^1 dh_0 dh_1 \exp \left[-\frac{2\pi}{\tau} F(h_0, h_1) \right]. \quad (2.25)$$

We consider about this exponential integral in the zero-temperature limit $\tau \rightarrow 0$.

3 Mean-field approximation with complex saddle points

In this section, we explain the mean-field approximation when the microscopic theory suffers from the sign problem [44].

3.1 Lefschetz-thimble methods and mean-field approximation

Here, we explain the general formalism to apply the mean-field approximation when the theory suffers from the sign problem. That is, we consider to apply the mean-field approximation to the path integral

$$Z = \int \mathcal{D}\phi \exp(-S[\phi]), \quad (3.1)$$

where the classical action $S[\phi]$ takes complex values. To consider the mean-field approximation, we introduce the order-parameter operator $O[\phi]$, and define the constrained free energy density [63, 64] by

$$F(\Phi) = -\frac{1}{V} \ln \left[\int \mathcal{D}\phi \exp(-S[\phi]) \delta(O[\phi] - \Phi) \right]. \quad (3.2)$$

If $S[\phi]$ is real, then $F[\Phi]$ is also real and one can compute phase diagram by taking the minimum of $F(\Phi)$. However, if there is the sign problem, the free energy $F(\Phi)$ is complex, and its physical meaning becomes unclear [65, 66].

The partition function and the constrained free energy is related by

$$Z = \int_{\mathcal{M}} d\Phi \exp(-VF(\Phi)), \quad (3.3)$$

where \mathcal{M} is the target space of order parameters Φ . This corresponds to (2.25) in our model, where $\Phi = (h_0, h_1)$ and $\mathcal{M} = (\mathbb{R}/\mathbb{Z})^2$. In the mean-field approximation, we would like to evaluate this integral in the limit $V \rightarrow \infty$ using the saddle-point approximation. Since $F[\Phi]$ is complex, this integral is an multi-dimensional oscillatory integral, and we need a technique to treat it. Here, we use the knowledge of the hyperasymptotic analysis [11–13], which is recently used for the study of sign problem of the lattice Monte Carlo simulation and known as the Lefschetz-thimble method [33–55].

The basic idea is to deform the integration contour \mathcal{M} into steepest descent cycles inside its complexified space $\mathcal{M}_{\mathbb{C}}$ by using the Cauchy theorem when $F(\Phi)$ is holomorphic. We denote the holomorphic coordinate of $\mathcal{M}_{\mathbb{C}}$ as $\Phi = (z^1, \dots, z^n)$, and the set of saddle points as

$$\Sigma = \{z_{\sigma}\} := \left\{ \frac{\partial F}{\partial z^i} = 0 \right\}. \quad (3.4)$$

Using the Kähler metric on $\mathcal{M}_{\mathbb{C}}$, $ds^2 = g_{i\bar{j}} dz^i \otimes d\bar{z}^{\bar{j}}$, we define the gradient flow by

$$\frac{dz^i}{dt} = g^{i\bar{j}} \overline{\left(\frac{\partial F(z)}{\partial z^{\bar{j}}} \right)}. \quad (3.5)$$

As an important property of this differential equation, we have

$$\frac{dF}{dt} = |\partial F|^2 \geq 0. \quad (3.6)$$

Therefore, along the flow line, the real part of the free energy increases while its imaginary part stays constant. This means that we can define the steepest descent and ascent cycles associated with each saddle point z_σ by this gradient flow. Using solutions of the gradient flow $z(t)$, they are defined as

$$\mathcal{J}_\sigma = \{z(0) \mid z(t) \rightarrow z_\sigma, t \rightarrow -\infty\}, \quad \mathcal{K}_\sigma = \{z(0) \mid z(t) \rightarrow z_\sigma, t \rightarrow +\infty\}. \quad (3.7)$$

\mathcal{J}_σ and \mathcal{K}_σ are called Lefschetz thimble and dual thimble, respectively. They are dual quantities in terms of the intersection pairing $\langle \cdot, \cdot \rangle$, i.e., $\langle \mathcal{J}_\sigma, \mathcal{K}_\tau \rangle = \delta_{\sigma\tau}$, which means that one can decompose \mathcal{M} in terms of \mathcal{J}_σ as

$$\int_{\mathcal{M}} d\Phi \exp(-VF(\Phi)) = \sum_{\sigma \in \Sigma} \langle \mathcal{M}, \mathcal{K}_\sigma \rangle \int_{\mathcal{J}_\sigma} d^n z \exp(-VF(z)). \quad (3.8)$$

If all $\text{Re}(F(z_\sigma))$ are different with each other in the limit $V \rightarrow \infty$, we replace the integral by the saddle-point approximation, and we obtain at the leading order that

$$Z = \sum_{\sigma} \langle \mathcal{M}, \mathcal{K}_\sigma \rangle \exp(-VF(z_\sigma)). \quad (3.9)$$

We can summarize the necessary steps of the mean-field approximation with the sign problem as follows:

- Complexify the target space \mathcal{M} to $\mathcal{M}_{\mathbb{C}}$, and find the saddle points z_σ by solving the equation $\partial F = 0$ in $\mathcal{M}_{\mathbb{C}}$.
- Solve the gradient flow (3.5), and construct Lefschetz thimbles \mathcal{J}_σ and dual thimbles \mathcal{K}_σ .
- Pick up the saddle point z_σ that has the minimal free energy $\text{Re}(F(z_\sigma))$ with nonzero intersection number $\langle \mathcal{M}, \mathcal{K}_\sigma \rangle$.

3.2 Charge and complex conjugation for real-valued free energy

In Sec. 3.1, we explained the way to apply the Lefschetz thimble method to the mean-field calculations for the theory with the sign problem. However, since the free energy $F(z)$ is complex in general, it would not be clear if the mean-field free energy $F(z_\sigma)$ becomes real in the above procedure. Following Ref. [44], we explain that this is ensured under the charge conjugation of the original theory.

To explain it, we consider a fermionic system and denote the chemical potential dependence of the free energy explicitly as $F = F(\Phi, \mu)$. In many examples of the fermionic system at finite densities, unbalance between the fermion and anti-fermion numbers due to the chemical potential causes the sign problem, and the free energy satisfies

$$\overline{F(\Phi, \mu)} = F(\Phi, -\mu). \quad (3.10)$$

In order to relate $F(\Phi, -\mu)$ to the original one, we consider the charge conjugation C , which flips the sign of the chemical potential. Then, we have

$$\overline{F(\Phi, \mu)} = F(C \cdot \Phi, \mu). \quad (3.11)$$

Indeed, this is satisfied for Polyakov-loop extended Nambu–Jona-Lasinio model [67–69], heavy-dense quantum chromodynamics (QCD) [65, 66, 70–79], perturbative QCD with finite μ [80, 81], Thirring model at finite densities [48–52, 82] and also QED₂ in Sec. 2. Even after complexification, the anti-linear extension of the charge conjugation plays an important role,

$$z \mapsto C \cdot \bar{z}, \quad (3.12)$$

because

$$\overline{F(z, \mu)} = F(C \cdot \bar{z}, \mu). \quad (3.13)$$

This property is called the CK-symmetry of the complexified theory in Refs. [67, 68].

Under a certain condition of the Kähler metric and the charge conjugation, one can show that $C \cdot \bar{z}(t)$ satisfies the same equation (3.5) for any solutions $z(t)$ of the gradient flow [44]. Now, one can classify the set of saddle points z_σ into three cases,

$$\Sigma_{\text{CK}} = \{z_\sigma = C \cdot \bar{z}_\sigma\}, \quad \Sigma_\pm = \{\text{Im}F(z_\sigma) \gtrless 0\}. \quad (3.14)$$

We here notice that $F(z_\sigma)$ is real if the saddle-point is CK-invariant, $z_\sigma = C \cdot \bar{z}_\sigma$ ¹. If the mean-field theory is valid, then $F(z_\sigma)$ of the selected saddle point must be real. Therefore, if one can show or assumes the validity of the mean-field approximation, it is enough to consider the gradient flow (3.5) inside the CK-invariant hyperplane, and one can pick up the CK-invariant saddle point of the minimal free energy with nonzero intersection number $\langle \mathcal{M}, \mathcal{K}_\sigma \rangle$. We will see that this is the case for the sign problem of multi-flavor massless QED₂ in the zero-temperature limit.

4 Lefschetz-thimble calculus for multi-flavor massless QED₂

In this section, we consider the phase diagram of multi-flavor massless QED₂ at finite L and the zero-temperature limit $\beta \rightarrow \infty$. For this purpose, we compute the path integral (2.25) based on the Lefschetz-thimble method, and the mean-field calculation with the complex saddle points given in Sec. 3 turns out to be powerful for our purpose.

4.1 Complex saddle points of multi-flavor massless QED₂

We use the same symbol for the complexified toron fields, h_0 and h_1 . We define the Kähler metric on complex (h_0, h_1) space $(\mathbb{C}/\mathbb{Z})^2$ by

$$ds^2 = \tau^2 dh_0 \otimes d\bar{h}_0 + dh_1 \otimes d\bar{h}_1. \quad (4.1)$$

The gradient flow to be solved in this metric is given by

$$\frac{dh_0}{dt} = \frac{1}{\tau^2} \overline{\left(\frac{\partial F}{\partial h_0} \right)}, \quad \frac{dh_1}{dt} = \overline{\left(\frac{\partial F}{\partial h_1} \right)}, \quad (4.2)$$

¹If the theory has other discrete symmetries, such as parity, center symmetry, etc., then one can construct other CK-transformation by combining them with the charge and complex conjugation. In such cases, we call $z_\sigma \in \Sigma_{\text{CK}}$ if z_σ is invariant under one of them.

where the explicit form of the right hand sides is given as

$$\begin{aligned} \frac{\partial F}{\partial h_0} &= i\tau \sum_{a=1}^{N_f} \sum_{n=1}^{\infty} \left\{ \left(1 + e^{\frac{2\pi}{\tau}(n+h_1-1-\mu'_a)+2\pi i h_0} \right)^{-1} - \left(1 + e^{\frac{2\pi}{\tau}(n-h_1+\mu'_a)-2\pi i h_0} \right)^{-1} \right. \\ &\quad \left. + \left(1 + e^{\frac{2\pi}{\tau}(n-h_1-\mu'_a)+2\pi i h_0} \right)^{-1} - \left(1 + e^{\frac{2\pi}{\tau}(n+h_1-1+\mu'_a)-2\pi i h_0} \right)^{-1} \right\}, \end{aligned} \quad (4.3)$$

$$\begin{aligned} \frac{\partial F}{\partial h_1} &= 2N_f \left(h_1 - \frac{1}{2} \right) \\ &\quad + \sum_{a=1}^{N_f} \sum_{n=1}^{\infty} \left\{ \left(1 + e^{\frac{2\pi}{\tau}(n+h_1-1-\mu'_a)+2\pi i h_0} \right)^{-1} - \left(1 + e^{\frac{2\pi}{\tau}(n-h_1+\mu'_a)-2\pi i h_0} \right)^{-1} \right. \\ &\quad \left. - \left(1 + e^{\frac{2\pi}{\tau}(n-h_1-\mu'_a)+2\pi i h_0} \right)^{-1} + \left(1 + e^{\frac{2\pi}{\tau}(n+h_1-1+\mu'_a)-2\pi i h_0} \right)^{-1} \right\}. \end{aligned} \quad (4.4)$$

What we have to do for the Lefschetz-thimble method is to find the saddle points of F in the complexified (h_0, h_1) space. Therefore, from (4.3) and (4.4), we need to solve

$$\begin{aligned} \sum_{a=1}^{N_f} \sum_{n=1}^{\infty} \left\{ \left(1 + e^{\frac{2\pi}{\tau}(n+h_1-1-\mu'_a)+2\pi i h_0} \right)^{-1} - \left(1 + e^{\frac{2\pi}{\tau}(n-h_1+\mu'_a)-2\pi i h_0} \right)^{-1} \right\} &= -N_f \left(h_1 - \frac{1}{2} \right), \\ \sum_{a=1}^{N_f} \sum_{n=1}^{\infty} \left\{ \left(1 + e^{\frac{2\pi}{\tau}(n-h_1-\mu'_a)+2\pi i h_0} \right)^{-1} - \left(1 + e^{\frac{2\pi}{\tau}(n+h_1-1+\mu'_a)-2\pi i h_0} \right)^{-1} \right\} &= N_f \left(h_1 - \frac{1}{2} \right). \end{aligned} \quad (4.5)$$

By taking the zero-temperature limit $\tau \rightarrow 0$, one can simplify this saddle-point condition as follows. In the limit $\tau \rightarrow 0$, we notice that the summation over spatial momenta n is represented by the floor function,

$$\begin{aligned} &\sum_{n=1}^{\infty} \left\{ \left(1 + e^{\frac{2\pi}{\tau}(n+h_1-1-\mu'_a)+2\pi i h_0} \right)^{-1} - \left(1 + e^{\frac{2\pi}{\tau}(n-h_1+\mu'_a)-2\pi i h_0} \right)^{-1} \right\} \\ &\rightarrow \max(0, \lfloor 1 - \operatorname{Re}(h_1) + \mu'_a + \tau \operatorname{Im}(h_0) \rfloor) - \max(0, \lfloor \operatorname{Re}(h_1) - \mu'_a - \tau \operatorname{Im}(h_0) \rfloor) \\ &= \lfloor 1 - \operatorname{Re}(h_1) + \mu'_a + \tau \operatorname{Im}(h_0) \rfloor. \end{aligned} \quad (4.6)$$

Therefore, the saddle-point conditions (4.5) at $\tau \ll 1$ must be well approximated by

$$\sum_{a=1}^{N_f} \lfloor 1 - \operatorname{Re}(h_1) + \mu'_a + \tau \operatorname{Im}(h_0) \rfloor = -N_f \left(h_1 - \frac{1}{2} \right), \quad (4.7)$$

$$\sum_{a=1}^{N_f} \lfloor \operatorname{Re}(h_1) + \mu'_a + \tau \operatorname{Im}(h_0) \rfloor = N_f \left(h_1 - \frac{1}{2} \right). \quad (4.8)$$

Since the left hand sides of these equations are real and integers because they are left- and right-handed fermion numbers, so are the right hand sides. This claims that h_1 must be real and, especially²,

$$h_1 \in \left(\frac{1}{2} + \frac{1}{N_f} \mathbb{Z} \right) / \mathbb{Z}. \quad (4.9)$$

²If some arguments of the floor function converge to integers in $\tau \rightarrow 0$, complex saddle points with other h_1 's can exist. We shall find them by solving the gradient flow numerically inside the CK-invariant plane in

For further consideration on the saddle points, we need to specify the number of fermion flavors N_f . We will consider the case for $N_f = 1, 2$, and 3 in following subsections.

For the mean-field calculations, the computation of the free energy is also an important ingredient. In the limit $\tau \rightarrow 0$, one can find after a slightly technical computation that the free energy (2.24) also accepts the much simplified expression as

$$\begin{aligned}
F &= N_f \left(h_1 - \frac{1}{2} \right)^2 + \frac{1}{2} \sum_{a=1}^{N_f} \left\{ [1 - h_1 + \mu'_a + \tau \text{Im}(h_0)]^2 + [h_1 + \mu'_a + \tau \text{Im}(h_0)]^2 \right\} \\
&+ \left(h_1 - \frac{1}{2} \right) \sum_{a=1}^{N_f} \left([1 - h_1 + \mu'_a + \tau \text{Im}(h_0)] - [h_1 + \mu'_a + \tau \text{Im}(h_0)] \right) \\
&+ \sum_{a=1}^{N_f} (\tau i h_0 - \mu'_a) \left([1 - h_1 + \mu'_a + \tau \text{Im}(h_0)] + [h_1 + \mu'_a + \tau \text{Im}(h_0)] \right). \quad (4.10)
\end{aligned}$$

One should notice that h_0 dependence totally disappears in the vicinity of the complex saddle points satisfying (4.7) and (4.8). This is due to the charge neutrality condition on the torus;

$$\sum_{a=1}^{N_f} [1 - h_1 + \mu'_a + \tau \text{Im}(h_0)] + \sum_{a=1}^{N_f} [h_1 + \mu'_a + \tau \text{Im}(h_0)] = 0. \quad (4.11)$$

Then, we find that the imaginary part of the constrained free energy also disappears under that condition. This fact is remarkable because use of complex saddle points weakens the sign problem of the massless multi-flavor QED₂.

4.2 1-flavor case

Let us first consider the case $N_f = 1$. The saddle point condition for h_1 , (4.9), says that $h_1 = \frac{1}{2}$. Then, Eqs. (4.7) and (4.8) reduce to the single equation,

$$\left| \frac{1}{2} + \mu' + \tau \text{Im}(h_0) \right| = 0, \quad (4.12)$$

which can be trivially satisfied by choosing $\tau \text{Im}(h_0) = -\mu'$. This saddle-point condition says that both the left- and right-handed fermion densities are always zero for any chemical potential.

One can understand this result in an easier way. The chemical potential dependence of the free energy (2.24) can be written as

$$F(h_0, h_1, \mu) = F \left(h_0 + \frac{i}{\tau} \mu', h_1 \right). \quad (4.13)$$

Sec. 5. However, all of them turns out not to be selected as correct mean fields, since they do not have the minimal free energy with non-zero intersection number, and it is reasonable because the fermion numbers at those saddle points are not quantized even at the zero-temperature limit. Therefore, we neglect such subtle possibilities for a while.

Therefore, just by shifting h_0 as $h_0 - i\mu'/\tau$, the free energy becomes a real function, and the sign problem disappears. The partition function does not change under this continuous change of contours, so the chemical potential dependence does not appear in the single-flavor case.

4.3 2-flavor case

Let us next consider the case $N_f = 2$. The saddle-point condition (4.9) requires that $h_1 = \frac{1}{2}$ or $h_1 = 0$. For $h_1 = 0$, Eqs. (4.7) and (4.8) become

$$[1 + \mu'_1 + \tau \text{Im}(h_0)] + [1 + \mu'_2 + \tau \text{Im}(h_0)] = 1, \quad (4.14)$$

$$[\mu'_1 + \tau \text{Im}(h_0)] + [\mu'_2 + \tau \text{Im}(h_0)] = -1. \quad (4.15)$$

Since these two conditions are equivalent, and they can be satisfied by setting $\tau \text{Im}(h_0) = -\frac{1}{2}(\mu'_1 + \mu'_2)$ because $[x] + [-x] = -1$ for any $x \in \mathbb{R}$. Introducing the dimensionless isospin chemical potential by

$$\mu'_I = \mu'_1 - \mu'_2, \quad (4.16)$$

the free energy of this state is

$$F\left(-\frac{i}{2\tau}(\mu'_1 + \mu'_2), 0\right) = \frac{1}{2} + 2\left[\frac{\mu'_I}{2}\right] + 2\left[\frac{\mu'_I}{2}\right]^2 - \mu'_I\left(1 + 2\left[\frac{\mu'_I}{2}\right]\right). \quad (4.17)$$

For $h_0 = \frac{1}{2}$, Eqs. (4.7) and (4.8) become the single equation,

$$\left[\frac{1}{2} + \mu'_1 + \tau \text{Im}(h_0)\right] + \left[\frac{1}{2} + \mu'_2 + \tau \text{Im}(h_0)\right] = 0. \quad (4.18)$$

Again, this is satisfied by setting $\tau \text{Im}(h_0) = -\frac{1}{2}(\mu'_1 + \mu'_2)$, and the free energy becomes

$$F\left(-\frac{i}{2\tau}(\mu'_1 + \mu'_2), \frac{1}{2}\right) = 2\left[\frac{1}{2} + \frac{\mu'_I}{2}\right]^2 - 2\mu'_I\left[\frac{1}{2} + \frac{\mu'_I}{2}\right]. \quad (4.19)$$

Soon later, we shall show that both complex saddles have nonzero intersection number, and thus we must pick up a state with the lower free energy at a given chemical potential to determine the phase diagram. Figure 1a shows (4.17) and (4.19) with green and blue solid lines, respectively, and we can readily find that the phase transition at $\tau = 0$ happens when μ'_I is a half integer. The difference of the fermion numbers, $n_1 - n_2 = -2\frac{\partial}{\partial \mu'_I} F$, is shown in Fig. 1b. This result is consistent with the exact computation done in Ref. [7] and also with the result by the matrix product states in Ref. [10].

To complete our argument on the 2-flavor case, let us discuss the intersection numbers at the saddle points with $h_1 = 0$ and $h_1 = \frac{1}{2}$. It is important to notice that the saddle-point conditions for both cases are solved by $\tau \text{Im}(h_0) = -\frac{1}{2}(\mu'_1 + \mu'_2)$. Indeed, the free energy $F(h_0, h_1)$ becomes a real-valued function after the shift

$$h_0 \mapsto h_0 - i\frac{\mu'_1 + \mu'_2}{2}. \quad (4.20)$$

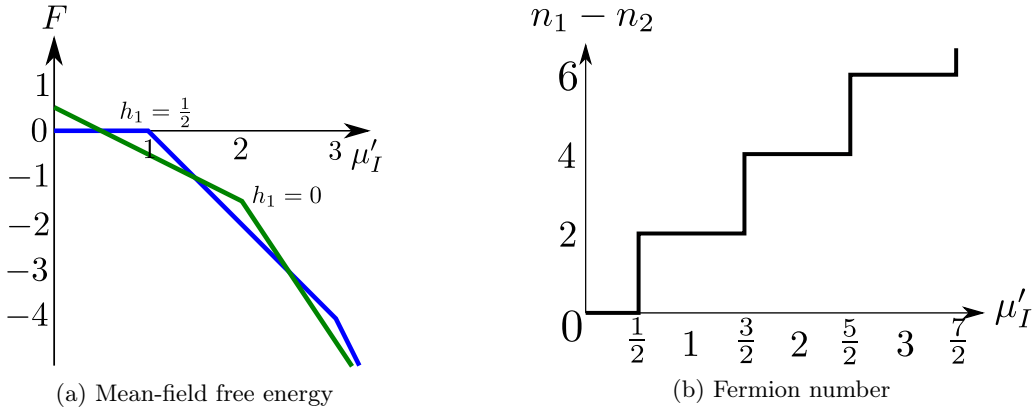


Figure 1. (a) Mean-field free energy at complex saddles with $h_1 = 0$ (green line) and $h_1 = \frac{1}{2}$ (blue line) as a function of $\mu'_I = \mu'_1 - \mu'_2$. (b) Behaviors of the difference of fermion numbers at $\tau = 0$ as a function of μ'_I .

The above two saddle points at $h_1 = 0, \frac{1}{2}$ correspond to local minimum of the real-valued free energy after this shift of h_0 , and thus the usual mean-field approximation becomes valid. This means that the intersection numbers of both saddle points are equal to 1:

$$\left(\mathbb{R}/\mathbb{Z} - i\frac{\mu'_1 + \mu'_2}{2}\right) \times (\mathbb{R}/\mathbb{Z}) = \mathcal{J}\left(-i\frac{\mu'_1 + \mu'_2}{2}, 0\right) + \mathcal{J}\left(-i\frac{\mu'_1 + \mu'_2}{2}, \frac{1}{2}\right), \quad (4.21)$$

when neglecting the consistently subdominant thimbles. This argument, however, also shows that the sign problem of two-flavor QED₂ can be eliminated just by the constant shift of integration variables.

4.4 3-flavor case

Let us consider the case $N_f = 3$ as a last example. This is the first nontrivial case, in which we cannot eliminate the sign problem by simply shifting the h_0 field. Without loss of generality, we can set $\mu_3 = 0$ by shift of h_0 . In the following, we solve the problem under this condition. The saddle-point condition for h_1 , (4.9) says that

$$h_1 = \frac{1}{2}, \frac{1}{2} \pm \frac{1}{3}. \quad (4.22)$$

We solve the saddle-point conditions for h_0 , (4.7) and (4.8), by separating cases.

1. We set $h_1 = \frac{1}{2}$. Introducing $y = \tau \text{Im}(h_0) + \frac{1}{2}$, the saddle-point condition at $T = 0$, (4.7) and (4.8), can be written as

$$[\mu'_1 + y] + [\mu'_2 + y] + [y] = 0. \quad (4.23)$$

To solve this condition, we set, for integers n and m ,

$$[\mu'_1 + y] = n, [\mu'_2 + y] = m, [y] = -n - m. \quad (4.24)$$

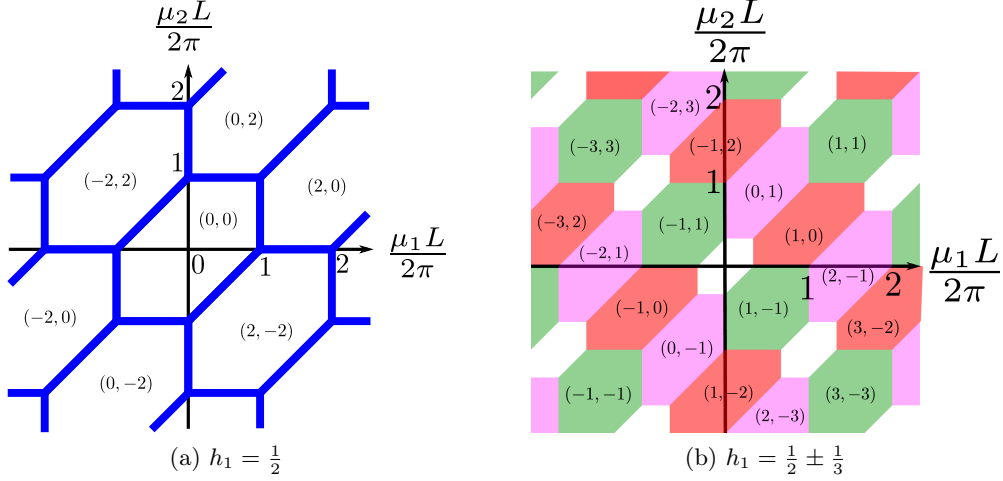


Figure 2. Classification of complex saddle points for the three-flavor case with $\mu_3 = 0$. In each figure, we set $h_1 = \frac{1}{2}$ and $h_1 = \frac{1}{6}, \frac{5}{6}$, respectively. We show the fermion numbers (n_1, n_2) in each region, and $n_3 = -n_1 - n_2$ due to the charge neutrality.

The region is surrounded by hexagon, which is the convex hull of the set of six points,

$$\left\{ \begin{array}{l} (2n + m - 1, n + 2m - 1), (2n + m, n + 2m - 1), (2n + m + 1, n + 2m), \\ (2n + m + 1, n + 2m + 1), (2n + m, n + 2m + 1), (2n + m - 1, n + 2m) \end{array} \right\}. \quad (4.25)$$

In Fig. 2a, we show the structure of these hexagons with corresponding fermion numbers $(n_1, n_2) = (2n, 2m)$. The free energy for this case becomes

$$F\left(h_0, \frac{1}{2}\right) = n^2 + m^2 + (-n - m)^2 - 2n\mu'_1 - 2m\mu'_2 - 2(-n - m)\mu'_3. \quad (4.26)$$

Here, we reinstate μ'_3 just for keep the expression symmetric.

2. We set $h_1 = \frac{1}{2} \pm \frac{1}{3}$. Setting $y = \tau \text{Im}(h_0) + \frac{1}{6}$, the conditions (4.7) and (4.8) become

$$\sum_{a=1}^3 [\mu'_a + y] = -1, \quad \sum_{a=1}^3 \left[\mu'_a + \frac{2}{3} + y \right] = 1. \quad (4.27)$$

Setting $\mu'_3 = 0$, we solve this condition by separating it into three cases.

- (a) We first consider the case

$$\left[\mu'_1 + \frac{2}{3} + y \right] = [\mu'_1 + y] + 1 = n + 1, \quad \left[\mu'_2 + \frac{2}{3} + y \right] = [\mu'_2 + y] = m. \quad (4.28)$$

The corresponding region becomes the hexagon, which is the convex hull of

$$\left\{ \begin{array}{l} (2n + m + \frac{1}{3}, n + 2m), (2n + m + 1, n + 2m), (2n + m + \frac{5}{3}, n + 2m + \frac{2}{3}), \\ (2n + m + \frac{5}{3}, n + 2m + 1), (2n + m + 1, n + 2m + 1), (2n + m + \frac{1}{3}, n + 2m + \frac{1}{3}) \end{array} \right\}. \quad (4.29)$$

(b) Next, consider the case

$$\left\lfloor \mu'_1 + \frac{2}{3} + y \right\rfloor = \lfloor \mu'_1 + y \rfloor = n, \quad \left\lfloor \mu'_2 + \frac{2}{3} + y \right\rfloor = \lfloor \mu'_2 + y \rfloor + 1 = m + 1. \quad (4.30)$$

The corresponding region becomes the hexagon, which is the convex hull of

$$\left\{ \begin{array}{l} (2n + m, n + 2m + \frac{1}{3}), (2n + m + \frac{1}{3}, n + 2m + \frac{1}{3}), (2n + m + 1, n + 2m + \frac{1}{3}), \\ (2n + m + 1, n + 2m + \frac{5}{3}), (2n + m + \frac{2}{3}, n + 2m + \frac{5}{3}), (2n + m, n + 2m + 1) \end{array} \right\}. \quad (4.31)$$

(c) Thirdly, consider the case

$$\left\lfloor \mu'_1 + \frac{2}{3} + y \right\rfloor = \lfloor \mu'_1 + y \rfloor + 1 = n + 1, \quad \left\lfloor \mu'_2 + \frac{2}{3} + y \right\rfloor = \lfloor \mu'_2 + y \rfloor + 1 = m + 1. \quad (4.32)$$

The corresponding region becomes the hexagon, which is the convex hull of

$$\left\{ \begin{array}{l} (2n + m + 1, n + 2m + 1), (2n + m + \frac{5}{3}, n + 2m + 1), (2n + m + 2, n + 2m + \frac{4}{3}), \\ (2n + m + 2, n + 2m + 2), (2n + m + \frac{4}{3}, n + 2m + 2), (2n + m + 1, n + 2m + \frac{5}{3}) \end{array} \right\}. \quad (4.33)$$

The result for $h_1 = \frac{1}{2} \pm \frac{1}{3}$ is summarized in Fig. 2b, where orange, pink and green regions correspond to the above cases 2a, 2b and 2c, respectively. The blank region of Fig. 2b means that there is no corresponding saddle point with $h_1 = \frac{1}{2} \pm \frac{1}{3}$ at those chemical potentials. The free energy becomes

$$\begin{aligned} F\left(h_0, \frac{1}{2} \pm \frac{1}{3}\right) &= -\frac{1}{3} + \frac{1}{2} \sum_{a=1}^3 \left(\left[\frac{5}{6} + \mu'_a + \tau \text{Im}(h_0) \right]^2 + \left[\frac{1}{6} + \mu'_a + \tau \text{Im}(h_0) \right]^2 \right) \\ &\quad - \sum_{a=1}^3 \mu'_a \left(\left[\frac{5}{6} + \mu'_a + \tau \text{Im}(h_0) \right] + \left[\frac{1}{6} + \mu'_a + \tau \text{Im}(h_0) \right] \right). \end{aligned} \quad (4.34)$$

We now have solved all the possible complex saddle points, and the corresponding free energies are computed. Since all the free energies are real and independent of τ , the mean-field calculation with those complex saddle points becomes exact in the zero-temperature limit $\tau \rightarrow 0$. As we have explained in Sec. 3, we need to compute the gradient flow (4.2) to construct the dual thimbles for this method, and select the phase with minimal free energy with nonzero intersection number. To streamline the discussion, however, we postpone the computation of the gradient flow to Sec. 5, and we *temporarily* assume that all the above complex saddle points contribute to the partition function in the formula (3.9). This temporal assumption shall be verified by solving the gradient flow in the next section.

We can readily compute the phase boundaries of the three-flavor massless QED₂ by using the information about complex saddle points. If there are several complex solutions at a given chemical potential by comparing Figs. 2a and 2b, we select the phase with the lower free energy. As a result, we obtain the phase boundaries given in Fig. 3. One can explicitly compare this result with the exact computation done by Ref. [8] to find its correctness (see Figure 4 of Ref. [8]).

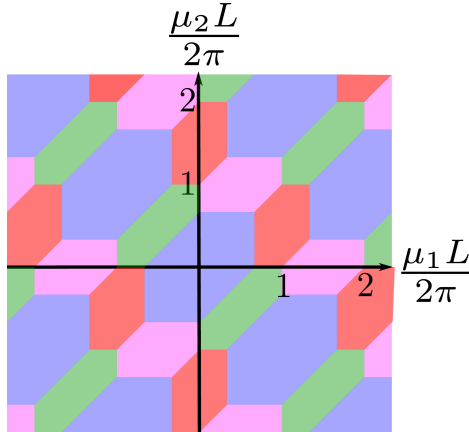


Figure 3. Phase boundaries of the three-flavor massless QED₂ at $T = 0$ and $\mu_3 = 0$. Inside blue hexagons, the phases in Fig. 2a are selected, i.e., $h_1 = \frac{1}{2}$. Hexagons with other colors represent the phase with $h_1 = \frac{1}{2} \pm \frac{1}{3}$, and the same color with Fig. 2b is used.

5 Gradient flow inside CK-invariant space

In order to check the intersection numbers of the dual thimbles, we solve the gradient flow numerically for three-flavor massless QED₂ in this section. We first emphasize the technical importance of the CK-transformation in order to visualize the gradient flow, and apply this technique to numerically solve the flow for $N_f = 3$. All the following procedures are valid also for larger N_f 's.

The big technical issue of the mean-field approximation with complex saddles is that we have to compute the intersection numbers between $(\mathbb{R}/\mathbb{Z})^2$ and dual thimbles \mathcal{K}_σ inside the complexified space $(\mathbb{C}/\mathbb{Z})^2$. Since it is impossible to draw figures in the four-dimensional manifold, we do not know a manifestly clear way to compute such quantities. The CK-transformation plays an important role to manage this issue for the massless QED₂.

Since the original theory has the symmetry under charge conjugation, one can construct the CK symmetry discussed in Sec. 3.2 [44, 67, 68],

$$\overline{F(h_0, h_1, \mu)} = F(-\overline{h_0}, \overline{h_1}, \mu). \quad (5.1)$$

Especially if $\text{Re}(h_0) = 0$ and $\text{Im}(h_1) = 0$, every physical quantity becomes real. One can also notice that the saddle points obtained in the previous section satisfy this restriction. Therefore, in the following, we solve the gradient flow under the condition

$$h_0 = iy/\tau, \quad h_1 = x, \quad (5.2)$$

with real x and y . Indeed, if one starts the gradient flow from a generic point inside the CK-invariant plane, then the flow line lies inside the CK-invariant plane [44]. The gradient

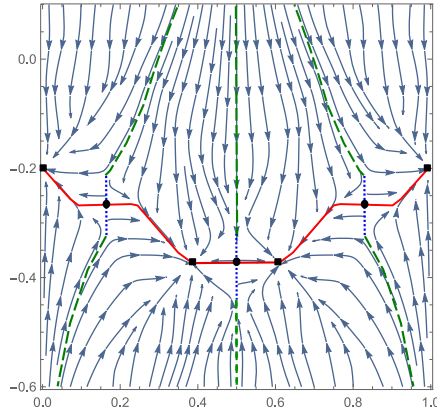


Figure 4. Gradient flow in the CK-invariant plane $\text{Re}(h_1) - \tau \text{Im}(h_0)$ at $(\mu'_1, \mu'_2) = (0.75, 0.2)$ and $\tau = 0.1$, and the schematic illustration of Lefschetz thimbles. Black blobs show the saddle points in the previous section, and black squares show other subdominant saddles. Blue dotted lines show the set of approximate saddle points. Red solid lines are Lefschetz thimbles \mathcal{J}_σ , and green dashed lines are parts of dual thimbles \mathcal{K}_σ connecting to the line segment of approximate saddles.

flow inside the CK-invariant plane obeys

$$\begin{aligned} \frac{dx}{dt} = & 2N_f \left(x - \frac{1}{2} \right) \\ & + \sum_{a=1}^{N_f} \sum_{n=1}^{\infty} \left\{ \left(1 + e^{\frac{2\pi}{\tau}(n+x-1-\mu'_a-y)} \right)^{-1} - \left(1 + e^{\frac{2\pi}{\tau}(n-x+\mu'_a+y)} \right)^{-1} \right. \\ & \left. - \left(1 + e^{\frac{2\pi}{\tau}(n-x-\mu'_a-y)} \right)^{-1} + \left(1 + e^{\frac{2\pi}{\tau}(n+x-1+\mu'_a+y)} \right)^{-1} \right\}, \end{aligned} \quad (5.3)$$

$$\begin{aligned} \frac{dy}{dt} = & - \sum_{a=1}^{N_f} \sum_{n=1}^{\infty} \left\{ \left(1 + e^{\frac{2\pi}{\tau}(n+x-1-\mu'_a-y)} \right)^{-1} - \left(1 + e^{\frac{2\pi}{\tau}(n-x+\mu'_a+y)} \right)^{-1} \right. \\ & \left. + \left(1 + e^{\frac{2\pi}{\tau}(n-x-\mu'_a-y)} \right)^{-1} - \left(1 + e^{\frac{2\pi}{\tau}(n+x-1+\mu'_a+y)} \right)^{-1} \right\}. \end{aligned} \quad (5.4)$$

We can now visualize the gradient flow inside the CK-invariant plane to compute the non-trivial quantities, intersection numbers. We numerically solve this equation to find out the structure of the gradient flow for the case $N_f = 3$, and judge the contribution to the free energy from complex saddle points.

We show the gradient flow and the schematic illustration of Lefschetz and dual thimbles in Fig. 4 at $(\mu'_1, \mu'_2) = (0.75, 0.2)$. The horizontal axis represents $x = \text{Re}(h_1)$, and the vertical axis does $y = \tau \text{Im}(h_0)$. We can find black blobs at $h_1 = \frac{1}{2}, \frac{1}{2} \pm \frac{1}{3}$, and they are saddle points computed in Sec. 4.4. There are blue dotted line segments through those saddles, which consist of approximate saddles at $\tau = 0.1$. This is because the saddle-point condition at $\tau = 0$, (4.7) and (4.8), does not designate the specific value of $\tau \text{Im}(h_0)$. At sufficiently low temperatures, the set of approximate saddle points form a line segment. The line segment of approximate saddles separate gradient flows, which moves almost horizontally towards right and left, and the flow lines emanating from it form a diamond-like shape.

Black squares show subdominant saddles, at which h_1 is not appropriately quantized as (4.22), and they are irrelevant in the mean-field calculation.

We can now comment on when the sign problem of the reweighting is severe. Only inside the diamond-shaped regions, overall number density vanishes, $\sum_{a=1}^3 n_a = 0$, and the sign problem along the h_0 -integration becomes absent. Therefore, if the real axis is away from the diamond-shaped region of the dominant saddle in Fig. 4, the conventional reweighting suffers from the severe sign problem. We can solve this problem by deforming the integration contours to Lefschetz thimbles.

The existence of the line segment of approximate saddles, however, makes it difficult to solve the gradient flow with good accuracy especially around the saddle points. This brings us the numerical problem to compute the Lefschetz thimbles \mathcal{J}_σ and dual thimbles \mathcal{K}_σ . However, what we need for the mean-field calculation with complex saddle points is the intersection number between the original integration cycle and dual thimbles \mathcal{K}_σ . Since the intersection number is a topological quantity, we do not need to compute \mathcal{K}_σ exactly, and we can approximate \mathcal{K}_σ as the line segment that contains z_σ and the flow sucked into the edges of the line segment. In Fig. 4, we show this approximate Lefschetz thimbles \mathcal{J}_σ by red solid lines, and the approximate dual thimbles \mathcal{K}_σ by green dashed lines combined with blue dotted lines. That is, if the line segment or the flow line sucked into the line segment intersects with the real axis, we must take the complex saddle into the Lefschetz thimble decomposition of the partition function.

This confirms that all the saddle points discussed in Sec. 4 contribute, and it justifies the mean-field calculation done in the previous section. Therefore, the phase boundaries for $N_f = 3$ given in Fig. 3 are exact at the zero-temperature $\tau = 0$.

6 Conclusion and perspective

We show that the mean-field approximation with complex saddle points gives the rigorous result on the phase structure of multi-flavor massless QED₂ at zero temperature and finite densities. We derive the saddle-point condition and concretely solve it for $N_f = 1, 2$, and 3 cases. By computing the gradient flow, we check the intersection number to list up the candidates of complex mean fields, and draw the phase diagram by comparing the mean-field free energies with nonzero intersection numbers.

Multi-flavor massless QED₂ suffers from the sign problem, and the conventional reweighting technique does not work for general large chemical potentials. We have shown that the Lefschetz-thimble method completely solves this problem at $T = 0$ for all the chemical potentials: After deforming the integration path into the complex space using the gradient flow, we can use the saddle-point method and the reweighting factor becomes consistent with 1. This means that the lattice Monte Carlo simulation on Lefschetz thimbles solves the exponential complexity of multi-flavor massless QED₂ at finite densities.

We would like to emphasize that this is highly nontrivial result. Indeed, there is an example of the fermion sign problem, the one-site Hubbard model, where the exponential complexity does remain even after the deformation of the integration path with the gradient flow [48]. In that example, complex zeros of the fermion determinant separate the original

integration cycle into multiple Lefschetz thimbles, and the summing up them gives an exponentially small reweighting factor in terms of the inverse temperature β . Both one-site Hubbard model and multi-flavor massless QED₂ are strongly-coupled fermionic systems, and they have the first-order phase transition induced by jumps of the fermion number. Why do these examples have the big difference in the Lefschetz-thimble approach?

In the one-site Hubbard model [48], there are infinitely many Lefschetz thimbles that contribute in the zero-temperature limit. Integration on each Lefschetz thimble at the saddle point z_σ is represented by $\exp(-\beta F(z_\sigma))$ in our notation, and the difference of the free energy $\beta(F(z_\sigma) - F(z_\tau))$ remains finite in the limit $\beta \rightarrow \infty$. This means that each Lefschetz-thimble integral gives a comparable contribution, and the interference among them affects significantly in the one-site Hubbard model. On the other hand, $F(z_\sigma)$'s in the multi-flavor massless QED₂ are independent of β , and thus $\beta(F(z_\sigma) - F(z_\tau)) \rightarrow \pm\infty$ in the limit $\beta \rightarrow \infty$. One of the Lefschetz thimbles dominate the others, and the destructive interference does not occur in massless QED₂.

Another speculative remark is that the charge neutrality condition (4.11) at the saddle point plays an important role to eliminate the sign problem in multi-flavor massless QED₂. In this model, the unbalance of oppositely charged particles creates the sign problem when integrating over the phase of the temporal Wilson loop, h_0 , because of the violation of charge neutrality at each real configuration. Use of the complexified fields makes the charge neutrality manifest, and the h_0 dependence of the free energy totally disappears in the vicinity of the complex saddle points. It is an important future study to understand what is a consequence of the color neutrality condition of other QCD-like gauge theories.

As a final remark, let us comment on the limitation of this study when we discuss the QCD sign problem. One of the biggest difference between massless QED₂ and the chiral limit of QCD is the property of the chiral symmetry. In QED₂, the chiral symmetry is broken by the axial anomaly, and the massless Nambu–Goldstone boson does not appear. Indeed, the spontaneous symmetry breaking of the continuous symmetry is forbidden in $(1+1)$ -dimensional field theories [83, 84]. On the other hand, QCD has the spontaneous chiral symmetry breaking, and massless pions exist. The existence of charged massless pions gives the big obstacle when applying the conventional reweighting technique to the sign problem of QCD at the zero temperature and finite density, which causes the early-onset problem of baryon number densities at half of the pion mass [85–95]. It is not yet known whether the massless pions bring any difficulties to the Lefschetz-thimble approach, and it cannot be discussed with massless QED₂ because of the different origin of chiral symmetry breaking. To identify the consequence of the chiral symmetry breaking to the Lefschetz thimbles must become a benchmark in the future study on applications of Lefschetz thimbles to the sign problem.

Acknowledgments

Y.T. is financially supported by Special Postdoctoral Researchers program of RIKEN. M.T. is supported in part by the JSPS Grant-in-Aid for Scientific Research, Grant No.16K05357.

References

- [1] E. Y. Loh, J. E. Gubernatis, R. T. Scalettar, S. R. White, D. J. Scalapino, and R. L. Sugar, “Sign problem in the numerical simulation of many-electron systems,” *Phys. Rev. B* **41** (May, 1990) 9301–9307.
- [2] G. G. Batrouni and P. de Forcrand, “The Fermion sign problem: A New decoupling transformation, and a new simulation algorithm,” *Phys. Rev. B* **48** (1993) 589, [arXiv:cond-mat/9211009 \[cond-mat\]](#).
- [3] S. Muroya, A. Nakamura, C. Nonaka, and T. Takaishi, “Lattice QCD at finite density: An Introductory review,” *Prog. Theor. Phys.* **110** (2003) 615–668, [arXiv:hep-lat/0306031 \[hep-lat\]](#).
- [4] J. S. Schwinger, “Gauge Invariance and Mass,” *Phys. Rev.* **125** (1962) 397–398.
- [5] J. S. Schwinger, “Gauge Invariance and Mass. 2.,” *Phys. Rev.* **128** (1962) 2425–2429.
- [6] R. Narayanan, “QED at a finite chemical potential,” *Phys. Rev.* **D86** (2012) 087701, [arXiv:1206.1489 \[hep-lat\]](#).
- [7] R. Narayanan, “Two flavor massless Schwinger model on a torus at a finite chemical potential,” *Phys. Rev.* **D86** (2012) 125008, [arXiv:1210.3072 \[hep-th\]](#).
- [8] R. Lohmayer and R. Narayanan, “Phase structure of two-dimensional QED at zero temperature with flavor-dependent chemical potentials and the role of multidimensional theta functions,” *Phys. Rev.* **D88** no. 10, (2013) 105030, [arXiv:1307.4969 \[hep-th\]](#).
- [9] C. Gatttringer, T. Kloiber, and V. Sazonov, “Solving the sign problems of the massless lattice Schwinger model with a dual formulation,” *Nucl. Phys.* **B897** (2015) 732–748, [arXiv:1502.05479 \[hep-lat\]](#).
- [10] M. C. Bañuls, K. Cichy, J. I. Cirac, K. Jansen, and S. Kühn, “Density induced phase transitions in QED₂ - A study with matrix product states,” [arXiv:1611.00705 \[hep-lat\]](#).
- [11] F. Pham, “Vanishing homologies and the n variable saddlepoint method,” in *Proc. Symp. Pure Math*, vol. 40.2, pp. 319–333. AMS, 1983.
- [12] D. Kaminski, “Exponentially improved stationary phase approximations for double integrals,” *Methods and Appl. of Analysis* **1** (1994) 44–56.
- [13] C. J. Howls, “Hyperasymptotics for multidimensional integrals, exact remainder terms and the global connection problem,” *Proc. R. Soc. A* **453** no. 1966, (1997) 2271–2294.
- [14] E. Witten, “Analytic Continuation Of Chern-Simons Theory,” in *Chern-Simons Gauge Theory: 20 Years After*, vol. 50, pp. 347–446. AMS/IP Stud. Adv. Math., 2010. [arXiv:1001.2933 \[hep-th\]](#).
- [15] E. Witten, “A New Look At The Path Integral Of Quantum Mechanics,” [arXiv:1009.6032 \[hep-th\]](#).
- [16] D. Harlow, J. Maltz, and E. Witten, “Analytic Continuation of Liouville Theory,” *JHEP* **1112** (2011) 071, [arXiv:1108.4417 \[hep-th\]](#).
- [17] G. V. Dunne and M. Ünsal, “Resurgence and Trans-series in Quantum Field Theory: The CP(N-1) Model,” *JHEP* **1211** (2012) 170, [arXiv:1210.2423 \[hep-th\]](#).
- [18] G. Basar, G. V. Dunne, and M. Ünsal, “Resurgence theory, ghost-instantons, and analytic continuation of path integrals,” *JHEP* **1310** (2013) 041, [arXiv:1308.1108 \[hep-th\]](#).

- [19] A. Cherman, D. Dorigoni, and M. Ünsal, “Decoding perturbation theory using resurgence: Stokes phenomena, new saddle points and Lefschetz thimbles,” *JHEP* **10** (2015) 056, [arXiv:1403.1277 \[hep-th\]](#).
- [20] A. Cherman, P. Koroteev, and M. Ünsal, “Resurgence and Holomorphy: From Weak to Strong Coupling,” *J. Math. Phys.* **56** no. 5, (2015) 053505, [arXiv:1410.0388 \[hep-th\]](#).
- [21] D. Dorigoni, “An Introduction to Resurgence, Trans-Series and Alien Calculus,” [arXiv:1411.3585 \[hep-th\]](#).
- [22] F. David, “Nonperturbative effects in matrix models and vacua of two-dimensional gravity,” *Phys.Lett.* **B302** (1993) 403–410, [arXiv:hep-th/9212106 \[hep-th\]](#).
- [23] G. Felder and R. Riser, “Holomorphic matrix integrals,” *Nucl.Phys.* **B691** (2004) 251–258, [arXiv:hep-th/0401191 \[hep-th\]](#).
- [24] M. Marino, “Nonperturbative effects and nonperturbative definitions in matrix models and topological strings,” *JHEP* **12** (2008) 114, [arXiv:0805.3033 \[hep-th\]](#).
- [25] M. Mariño, “Lectures on non-perturbative effects in large N gauge theories, matrix models and strings,” *Fortsch. Phys.* **62** (2014) 455–540, [arXiv:1206.6272 \[hep-th\]](#).
- [26] R. Schiappa and R. Vaz, “The Resurgence of Instantons: Multi-Cut Stokes Phases and the Painleve II Equation,” *Commun. Math. Phys.* **330** (2014) 655–721, [arXiv:1302.5138 \[hep-th\]](#).
- [27] A. Behtash, T. Sulejmanpasic, T. Schäfer, and M. Ünsal, “Hidden Topological Angles in Path Integrals,” *Phys. Rev. Lett.* **115** no. 4, (2015) 041601, [arXiv:1502.06624 \[hep-th\]](#).
- [28] A. Behtash, E. Poppitz, T. Sulejmanpasic, and M. Ünsal, “The curious incident of multi-instantons and the necessity of Lefschetz thimbles,” *JHEP* **11** (2015) 175, [arXiv:1507.04063 \[hep-th\]](#).
- [29] S. Gukov, M. Marino, and P. Putrov, “Resurgence in complex Chern-Simons theory,” [arXiv:1605.07615 \[hep-th\]](#).
- [30] S. Gukov, “RG Flows and Bifurcations,” [arXiv:1608.06638 \[hep-th\]](#).
- [31] T. Fujimori, S. Kamata, T. Misumi, M. Nitta, and N. Sakai, “Nonperturbative contributions from complexified solutions in $\mathbb{C}P^{N-1}$ models,” *Phys. Rev.* **D94** no. 10, (2016) 105002, [arXiv:1607.04205 \[hep-th\]](#).
- [32] C. Kozçaz, T. Sulejmanpasic, Y. Tanizaki, and M. Ünsal, “Cheshire Cat resurgence, Self-resurgence and Quasi-Exact Solvable Systems,” [arXiv:1609.06198 \[hep-th\]](#).
- [33] **AuroraScience** Collaboration, M. Cristoforetti, F. Di Renzo, and L. Scorzato, “New approach to the sign problem in quantum field theories: High density QCD on a Lefschetz thimble,” *Phys. Rev. D* **86** (2012) 074506, [arXiv:1205.3996 \[hep-lat\]](#).
- [34] M. Cristoforetti, F. Di Renzo, A. Mukherjee, and L. Scorzato, “Monte Carlo simulations on the Lefschetz thimble: taming the sign problem,” *Phys. Rev. D* **88** (2013) 051501, [arXiv:1303.7204 \[hep-lat\]](#).
- [35] M. Cristoforetti, F. Di Renzo, G. Eruzzi, A. Mukherjee, C. Schmidt, L. Scorzato, and C. Torrero, “An efficient method to compute the residual phase on a Lefschetz thimble,” *Phys. Rev. D* **89** (2014) 114505, [arXiv:1403.5637 \[hep-lat\]](#).
- [36] G. Aarts, “Lefschetz thimbles and stochastic quantisation: Complex actions in the complex plane,” *Phys. Rev. D* **88** (2013) 094501, [arXiv:1308.4811 \[hep-lat\]](#).

- [37] H. Fujii, D. Honda, M. Kato, Y. Kikukawa, S. Komatsu, and T. Sano, “Hybrid Monte Carlo on Lefschetz thimbles - A study of the residual sign problem,” *JHEP* **1310** (2013) 147, [arXiv:1309.4371 \[hep-lat\]](#).
- [38] A. Mukherjee and M. Cristoforetti, “Lefschetz thimble Monte Carlo for many body theories: application to the repulsive Hubbard model away from half filling,” *Phys. Rev. B* **90** (2014) 035134, [arXiv:1403.5680 \[cond-mat.str-el\]](#).
- [39] G. Aarts, L. Bongiovanni, E. Seiler, and D. Sexty, “Some remarks on Lefschetz thimbles and complex Langevin dynamics,” *JHEP* **1410** (2014) 159, [arXiv:1407.2090 \[hep-lat\]](#).
- [40] Y. Tanizaki and T. Koike, “Real-time Feynman path integral with Picard–Lefschetz theory and its applications to quantum tunneling,” *Ann. Phys.* **351** (2014) 250, [arXiv:1406.2386 \[math-ph\]](#).
- [41] A. Cherman and M. Unsal, “Real-Time Feynman Path Integral Realization of Instantons,” [arXiv:1408.0012 \[hep-th\]](#).
- [42] Y. Tanizaki, “Lefschetz-thimble techniques for path integral of zero-dimensional $O(n)$ sigma models,” *Phys. Rev. D* **91** (2015) 036002, [arXiv:1412.1891 \[hep-th\]](#).
- [43] T. Kanazawa and Y. Tanizaki, “Structure of Lefschetz thimbles in simple fermionic systems,” *JHEP* **1503** (2015) 044, [arXiv:1412.2802 \[hep-th\]](#).
- [44] Y. Tanizaki, H. Nishimura, and K. Kashiwa, “Evading the sign problem in the mean-field approximation through Lefschetz-thimble path integral,” *Phys. Rev. D* **91** (2015) 101701, [arXiv:1504.02979 \[hep-th\]](#).
- [45] F. Di Renzo and G. Eruzzi, “Thimble regularization at work: from toy models to chiral random matrix theories,” *Phys. Rev. D* **92** (2015) 085030, [arXiv:1507.03858 \[hep-lat\]](#).
- [46] K. Fukushima and Y. Tanizaki, “Hamilton dynamics for the Lefschetz thimble integration akin to the complex Langevin method,” *Prog. Theor. Exp. Phys.* **2015** (2015) 111A01, [arXiv:1507.07351 \[hep-th\]](#).
- [47] S. Tsutsui and T. M. Doi, “An improvement in complex Langevin dynamics from a view point of Lefschetz thimbles,” *Phys. Rev.* **D94** (2016) 074009, [arXiv:1508.04231 \[hep-lat\]](#).
- [48] Y. Tanizaki, Y. Hidaka, and T. Hayata, “Lefschetz-thimble analysis of the sign problem in one-site fermion model,” *New J. Phys.* **18** (2016) 033002, [arXiv:1509.07146 \[hep-th\]](#).
- [49] H. Fujii, S. Kamata, and Y. Kikukawa, “Lefschetz thimble structure in one-dimensional lattice Thirring model at finite density,” *JHEP* **11** (2015) 078, [arXiv:1509.08176 \[hep-lat\]](#). [Erratum: *JHEP*02,036(2016)].
- [50] H. Fujii, S. Kamata, and Y. Kikukawa, “Monte Carlo study of Lefschetz thimble structure in one-dimensional Thirring model at finite density,” *JHEP* **12** (2015) 125, [arXiv:1509.09141 \[hep-lat\]](#).
- [51] A. Alexandru, G. Basar, and P. Bedaque, “Monte Carlo algorithm for simulating fermions on Lefschetz thimbles,” *Phys. Rev.* **D93** (2016) 014504, [arXiv:1510.03258 \[hep-lat\]](#).
- [52] T. Hayata, Y. Hidaka, and Y. Tanizaki, “Complex saddle points and the sign problem in complex Langevin simulation,” *Nucl. Phys.* **B911** (2016) 94–105, [arXiv:1511.02437 \[hep-lat\]](#).
- [53] A. Alexandru, G. Basar, P. F. Bedaque, G. W. Ridgway, and N. C. Warrington, “Sign

- problem and Monte Carlo calculations beyond Lefschetz thimbles,” *JHEP* **05** (2016) 053, [arXiv:1512.08764 \[hep-lat\]](#).
- [54] A. Alexandru, G. Basar, P. F. Bedaque, S. Vartak, and N. C. Warrington, “Monte Carlo Study of Real Time Dynamics on the Lattice,” *Phys. Rev. Lett.* **117** (2016) 081602, [arXiv:1605.08040 \[hep-lat\]](#).
- [55] A. Alexandru, G. Basar, P. F. Bedaque, G. W. Ridgway, and N. C. Warrington, “Monte Carlo calculations of the finite density Thirring model,” *Phys. Rev.* **D95** (2017) 014502, [arXiv:1609.01730 \[hep-lat\]](#).
- [56] C. K. Dumlu and G. V. Dunne, “The Stokes Phenomenon and Schwinger Vacuum Pair Production in Time-Dependent Laser Pulses,” *Phys. Rev. Lett.* **104** (2010) 250402, [arXiv:1004.2509 \[hep-th\]](#).
- [57] C. K. Dumlu and G. V. Dunne, “Interference Effects in Schwinger Vacuum Pair Production for Time-Dependent Laser Pulses,” *Phys. Rev. D* **83** (2011) 065028, [arXiv:1102.2899 \[hep-th\]](#).
- [58] C. K. Dumlu and G. V. Dunne, “Complex Worldline Instantons and Quantum Interference in Vacuum Pair Production,” *Phys. Rev. D* **84** (2011) 125023, [arXiv:1110.1657 \[hep-th\]](#).
- [59] P. V. Buividovich, G. V. Dunne, and S. N. Valgushev, “Complex Path Integrals and Saddles in Two-Dimensional Gauge Theory,” *Phys. Rev. Lett.* **116** no. 13, (2016) 132001, [arXiv:1512.09021 \[hep-th\]](#).
- [60] G. Álvarez, L. Martínez Alonso, and E. Medina, “Complex saddles in the Gross-Witten-Wadia matrix model,” *Phys. Rev.* **D94** no. 10, (2016) 105010, [arXiv:1610.09948 \[hep-th\]](#).
- [61] I. Sachs and A. Wipf, “Finite temperature Schwinger model,” *Helv. Phys. Acta* **65** (1992) 652–678, [arXiv:1005.1822 \[hep-th\]](#).
- [62] K. Langfeld and A. Wipf, “Fermi-Einstein condensation in dense QCD-like theories,” *Annals Phys.* **327** (2012) 994–1029, [arXiv:1109.0502 \[hep-lat\]](#).
- [63] C. Korthals Altes, “Constrained effective potential in hot QCD,” *Nucl.Phys.* **B420** (1994) 637–668, [arXiv:hep-th/9310195 \[hep-th\]](#).
- [64] R. Fukuda and E. Kyriakopoulos, “Derivation of the Effective Potential,” *Nucl.Phys.* **B85** (1975) 354.
- [65] A. Dumitru, R. D. Pisarski, and D. Zschiesche, “Dense quarks, and the fermion sign problem, in a SU(N) matrix model,” *Phys. Rev. D* **72** (2005) 065008, [arXiv:hep-ph/0505256 \[hep-ph\]](#).
- [66] K. Fukushima and Y. Hidaka, “A Model study of the sign problem in the mean-field approximation,” *Phys. Rev. D* **75** (2007) 036002, [arXiv:hep-ph/0610323 \[hep-ph\]](#).
- [67] H. Nishimura, M. C. Ogilvie, and K. Pangeni, “Complex saddle points in QCD at finite temperature and density,” *Phys. Rev. D* **90** (2014) 045039, [arXiv:1401.7982 \[hep-ph\]](#).
- [68] H. Nishimura, M. C. Ogilvie, and K. Pangeni, “Complex Saddle Points and Disorder Lines in QCD at finite temperature and density,” *Phys. Rev. D* **91** no. 5, (2015) 054004, [arXiv:1411.4959 \[hep-ph\]](#).
- [69] K. Fukushima, “Chiral effective model with the Polyakov loop,” *Phys.Lett.* **B591** (2004) 277–284, [arXiv:hep-ph/0310121 \[hep-ph\]](#).

- [70] C. Alexandrou, A. Borici, A. Feo, P. de Forcrand, A. Galli, F. Jegerlehner, and T. Takaishi, “The Deconfinement phase transition in one flavor QCD,” *Phys.Rev.* **D60** (1999) 034504, [arXiv:hep-lat/9811028 \[hep-lat\]](#).
- [71] J. Condezza and C. E. Detar, “Potts flux tube model at nonzero chemical potential,” *Phys.Rev.* **D61** (2000) 074023, [arXiv:hep-lat/9910028 \[hep-lat\]](#).
- [72] M. G. Alford, S. Chandrasekharan, J. Cox, and U. Wiese, “Solution of the complex action problem in the Potts model for dense QCD,” *Nucl.Phys.* **B602** (2001) 61–86, [arXiv:hep-lat/0101012 \[hep-lat\]](#).
- [73] T. Banks and A. Ukawa, “Deconfining and Chiral Phase Transitions in Quantum Chromodynamics at Finite Temperature,” *Nucl.Phys.* **B225** (1983) 145.
- [74] R. D. Pisarski, “Quark gluon plasma as a condensate of SU(3) Wilson lines,” *Phys.Rev.* **D62** (2000) 111501, [arXiv:hep-ph/0006205 \[hep-ph\]](#).
- [75] A. Dumitru and R. D. Pisarski, “Event-by-event fluctuations from decay of a Polyakov loop condensate,” *Phys.Lett.* **B504** (2001) 282–290, [arXiv:hep-ph/0010083 \[hep-ph\]](#).
- [76] O. Akerlund, P. de Forcrand, and T. Rindlisbacher, “Oscillating propagators in heavy-dense QCD,” *JHEP* **10** (2016) 055, [arXiv:1602.02925 \[hep-lat\]](#).
- [77] T. Hirakida, H. Kouno, J. Takahashi, and M. Yahiro, “Interplay between sign problem and Z_3 symmetry in three-dimensional Potts models,” *Phys. Rev.* **D94** no. 1, (2016) 014011, [arXiv:1604.02977 \[hep-lat\]](#).
- [78] I. Bender, T. Hashimoto, F. Karsch, V. Linke, A. Nakamura, M. Plewnia, I. O. Stamatescu, and W. Wetzel, “Full QCD and QED at finite temperature and chemical potential,” *Nucl. Phys. Proc. Suppl.* **26** (1992) 323–325.
- [79] T. C. Blum, J. E. Hetrick, and D. Toussaint, “High density QCD with static quarks,” *Phys. Rev. Lett.* **76** (1996) 1019–1022, [arXiv:hep-lat/9509002 \[hep-lat\]](#).
- [80] S. Hands, T. J. Hollowood, and J. C. Myers, “QCD with Chemical Potential in a Small Hyperspherical Box,” *JHEP* **07** (2010) 086, [arXiv:1003.5813 \[hep-th\]](#).
- [81] U. Reinosa, J. Serreau, and M. Tissier, “Perturbative study of the QCD phase diagram for heavy quarks at nonzero chemical potential,” *Phys. Rev. D* **92** no. 2, (2015) 025021, [arXiv:1504.02916 \[hep-th\]](#).
- [82] J. M. Pawłowski and C. Zielinski, “Thirring model at finite density in 0+1 dimensions with stochastic quantization: Crosscheck with an exact solution,” *Phys. Rev. D* **87** (2013) 094503, [arXiv:1302.1622 \[hep-lat\]](#).
- [83] S. R. Coleman, “There are no Goldstone bosons in two-dimensions,” *Commun. Math. Phys.* **31** (1973) 259–264.
- [84] N. D. Mermin and H. Wagner, “Absence of ferromagnetism or antiferromagnetism in one-or two-dimensional isotropic Heisenberg models,” *Phys. Rev. Lett.* **17** (1966) 1133.
- [85] P. E. Gibbs, “Lattice Monte Carlo Simulations of QCD at Finite Baryonic Density,” *Phys. Lett.* **B182** (1986) 369–372.
- [86] P. E. Gibbs, “The Fermion Propagator Matrix in Lattice QCD,” *Phys. Lett.* **B172** (1986) 53–61.
- [87] I. M. Barbour, S. E. Morrison, E. G. Klepfish, J. B. Kogut, and M.-P. Lombardo, “The

- Critical points of strongly coupled lattice QCD at nonzero chemical potential,” *Phys. Rev.* **D56** (1997) 7063–7072, [arXiv:hep-lat/9705038](#) [[hep-lat](#)].
- [88] I. M. Barbour, S. E. Morrison, E. G. Klepfish, J. B. Kogut, and M.-P. Lombardo, “Results on finite density QCD,” *Nucl. Phys. Proc. Suppl.* **60A** (1998) 220–234, [arXiv:hep-lat/9705042](#) [[hep-lat](#)].
- [89] M. A. Stephanov, “Random matrix model of QCD at finite density and the nature of the quenched limit,” *Phys. Rev. Lett.* **76** (1996) 4472–4475, [arXiv:hep-lat/9604003](#) [[hep-lat](#)].
- [90] T. D. Cohen, “Functional integrals for QCD at nonzero chemical potential and zero density,” *Phys. Rev. Lett.* **91** (2003) 222001, [arXiv:hep-ph/0307089](#) [[hep-ph](#)].
- [91] K. Splittorff and J. J. M. Verbaarschot, “Phase of the Fermion Determinant at Nonzero Chemical Potential,” *Phys. Rev. Lett.* **98** (2007) 031601, [arXiv:hep-lat/0609076](#) [[hep-lat](#)].
- [92] K. Splittorff and J. J. M. Verbaarschot, “The QCD Sign Problem for Small Chemical Potential,” *Phys. Rev.* **D75** (2007) 116003, [arXiv:hep-lat/0702011](#) [[HEP-LAT](#)].
- [93] A. Cherman, M. Hanada, and D. Robles-Llana, “Orbifold equivalence and the sign problem at finite baryon density,” *Phys. Rev. Lett.* **106** (2011) 091603, [arXiv:1009.1623](#) [[hep-th](#)].
- [94] Y. Hidaka and N. Yamamoto, “No-Go Theorem for Critical Phenomena in Large- N_c QCD,” *Phys. Rev. Lett.* **108** (2012) 121601, [arXiv:1110.3044](#) [[hep-ph](#)].
- [95] **XQCD-J** Collaboration, K. Nagata, S. Motoki, Y. Nakagawa, A. Nakamura, and T. Saito, “Towards extremely dense matter on the lattice,” *Prog. Theor. Exp. Phys.* **2012** (2012) 01A103, [arXiv:1204.1412](#) [[hep-lat](#)].